Theses and Dissertations                                                     Graduate School

2017

# Electronic and Structural Study of the Reactivity of Cu+ with CO, H2O, O2, N2 and their Mixture

Cara M. Frame
*Virginia Commonwealth University*

# Electronic and Structural Study of the Reactivity of $Cu^+$ with $CO$, $H_2O$, $O_2$, $N_2$ and their Mixture

A thesis submitted in partial fulfillment of the requirements for the degree of Master of Science

at Virginia Commonwealth University.

by

**Cara Mackenzie Frame**

B.S. Physics, University of Maryland, Baltimore County, 2007

Director: **Dr. J. Ulises Reveles**

Assistant Professor, Department of Physics

Virginia Commonwealth University

Richmond, Virginia

May 9, 2017

# Acknowledgements

First of all, I would like to thank my adviser, Dr. J. Ulises Reveles for accepting me as a student, and especially for being patient, helpful, and constantly supportive over the two years we worked together. I would also like to express my gratitude to the entire faculty and staff of the VCU Physics Department, who have made it into such a welcoming place for all students and a great learning environment. Finally, I want to thank my family and friends, particularly my parents, Kay and Rodney Frame, and my husband Riadh Bentorki, for supporting me, loving me, and believing in me, in good times and bad.

# Abstract

A detailed theoretical study of the gas phase reactivity of copper cation ($Cu^+$) with $CO$, $H_2O$, $O_2$, $N_2$ and their mixture was performed and compared to experimental results to determine the ability of $Cu^+$ to act as a low-temperature catalyst for $CO$ oxidation. It was found that $Cu^+$ binds strongest to $CO$, followed by $H_2O$, $N_2$, and $O_2$, strongly interacting with each species until reaching saturation at a maximum of four ligands. It was also found that a single $Cu^+$ cannot by itself activate the $O_2$ molecule as small copper cluster anions can, leading to $CO_2$ formation Nevertheless, since moisture and impurities on the surface of a catalyst can modify its chemical activity, it is important to understand at the atomic level the interaction between the active site ($Cu^+$) and the binding molecules in order to help to identify intermediates and key reaction steps that control the reactivity and catalytic activity.

# Table of Contents

# List of Tables

# List of Figures

# Chapter 1. Introduction

## 1.1 CO Catalysis

Carbon monoxide ($CO$) is a colorless, odorless gas that is a common byproduct of incomplete fuel combustion [1] via the following reaction [2]:

$$C_xH_y + O_2 \rightarrow CO_2 + CO + H_2O + H_2 \tag{1}$$
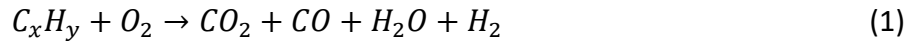
Carbon monoxide is therefore produced to some extent by all fuel-powered vehicles and essentially anything else that uses a hydrocarbon as a fuel, including generators, gas heaters, and propane grills. While carbon monoxide is in and of itself toxic to humans [1], an additional problem is that when present at ground level, $CO$ leads to the production of nitrogen dioxide ($NO_2$) and ozone ($O_3$) [3]. Both chemicals are toxic pollutants and ingredients of smog, which causes a wide variety of health problems for humans [4] including asthma [5] and lung cancer [6], among others. Anthropogenic ozone by itself, without including the effects of the particulate pollution also included in smog, has been estimated by various models to cause between 50,000 and 1,000,000 deaths a year worldwide, the majority of which occur in the densely-populated and highly-polluted regions of east and south Asia [4]. It is therefore essential to design fuel-burning equipment in such a way as to minimize the output of carbon monoxide.

Various methods are used to achieve this purpose, including, perhaps most importantly, designing equipment in such a way as to ensure a near-ideal mixture of oxygen is available for the combustion process to minimize the output of carbon monoxide in favor of carbon dioxide ($CO_2$) [7]. Being a long-lived greenhouse gas, carbon dioxide does cause many problems on its own. Notably, increases of $CO_2$ in the atmosphere are largely responsible for climate change [8].

However, given the more immediate harmful effects of carbon monoxide on the environment and human health, carbon dioxide is a preferable output.

However well-designed the combustion process is, *CO* is inevitably produced to some extent. This is the reason why most vehicles are equipped with catalytic converters, which are devices that convert carbon monoxide to carbon dioxide via the following reaction [7]:

$$CO + \frac{1}{2}O_2 \rightarrow CO_2 + \text{Energy} \qquad (2)$$

Most catalytic converters additionally reduce nitric oxide (*NO*) and nitrogen dioxide (*NO$_2$*) to *N$_2$* and *O$_2$* [7], although this process will not be discussed here. Because of the energy required to break the *O$_2$* bond, the carbon dioxide-producing reaction in equation 2 does not occur spontaneously without the presence of a catalyst. The catalyst reduces the activation energy for the reaction, and consequently, the temperature at which the reaction can occur [7].

There are two main mechanisms by which the catalysis of *CO* into *CO$_2$* is known to occur. In the Langmuir-Hinshelwood mechanism, both *O$_2$* and *CO* are coadsorbed on the surface of the catalyst [9]. The catalyst donates charge to the *O$_2$* molecule, which results in a stretching of the O-O bond. This is because the lowest unoccupied molecular orbital (LUMO) in *O$_2$* is an antibonding $\pi^*$ orbital [10]. Any charge added to *O$_2$* goes into this antibonding orbital and weakens the double bond holding the *O$_2$* together. This results in a lengthening of the bond and a reduction of the bond order, and one of the *O* atoms is able to break away and attach to *CO*, forming *CO$_2$*. In the Eley-Rideal mechanism, by contrast, only the *O$_2$* molecule directly adsorbs on the surface of the catalyst. The *CO* molecule then reacts with the activated *O$_2$* molecule directly in the gas phase without itself adsorbing on the surface of the catalyst [9]. The key to either

process is the activation of the $O_2$ molecule, without which the breaking of the $O_2$ bond cannot occur and $CO_2$ cannot be formed.

The bulk catalysts in catalytic converters work by the Langmuir-Hinshelwood mechanism [11], but $CO$ catalysis by both Langmuir-Hinshelwood and Eley-Rideal mechanisms are known to occur on small clusters [9].

If a suitable catalyst is not present, $CO$ indirectly aids in the formation of ozone ($O_3$) via the following series of reactions [3, 12]:

$$CO + O_2 + NO \rightarrow CO_2 + NO_2 \tag{3}$$

$$NO_2 + hv \rightarrow NO + O \tag{4}$$

$$O + O_2 \rightarrow O_3 \tag{5}$$

In the first step, carbon monoxide reacts with oxygen and nitric oxide to produce carbon dioxide and nitrogen dioxide. In the second step, nitrogen dioxide photodissociates due to sunlight to produce nitric oxide and single oxygen atoms. The single oxygen atoms then react with $O_2$ molecules to form ozone ($O_3$). Since sunlight is required to photodissociate the $NO_2$, ozone is produced in highest quantities during the daylight hours in summer and the amounts of ozone peak in late afternoon [14]. Both nitric oxide and nitrogen dioxide are byproducts of automobile emissions in addition to carbon monoxide [7]. This means that ozone is formed even without the presence of carbon monoxide. However, carbon monoxide increases the amount of ozone produced since it makes up a larger portion of vehicle exhaust than $NO_x$ by a factor of up to 20 [13]. Ozone is thermodynamically unstable and does eventually reduce to $O_2$ [15], but this process can take weeks [14] and $O_3$ is harmful in the meantime. Importantly, a catalytic converter

can prevent the production of ozone in favor of the relatively less immediately harmful carbon dioxide.

The catalysts used in catalytic converters are typically precious metals such as platinum, rhodium, and/or palladium [7]. These catalysts can, at the right temperature, reduce $CO$ and $NO_x$ emissions by up to 98% [7], but they do have a number of disadvantages. One of the primary drawbacks is that the precious metals used in them are extremely expensive. Platinum, for example, is approximately $975 per ounce [16]. Compare this to copper, which at $0.16 per ounce [17] is over 6000 times cheaper. Clearly, if copper or another cheaper metal could be used as a catalyst, it could significantly reduce the price of catalytic converters and make them more common, particularly in developing countries where cost is a bigger obstacle.

In addition, mining of precious metals causes detrimental environmental effects. More than half of the world's platinum and more than 85% of palladium is used in catalytic converters [18]. For example, the city of Norilsk, Russia, is one of the world's largest producers of platinum and palladium and is, as a result, considered to be one of the most polluted cities on earth [19]. Reducing the need for these metals in catalytic converters would decrease the amount of environmentally harmful mining.

Perhaps the most important drawback to current catalytic converters is that they require a high temperature to be effective. This means that vehicles emit a great deal of carbon monoxide during the first few minutes of operation after a cold start before the engine has had an opportunity to heat up sufficiently (typically to 300 - 400 ℃) [7]. A more ideal catalyst, capable of operating at ambient temperatures, would minimize the cold start problem and reduce harmful emissions.

A final disadvantage to current catalytic converters is that their effectiveness can be decreased or even completely ruined by the presence of contaminants in the system. Lead, for example, which used to be and still is in some countries added to gasoline as an anti-knocking agent, can completely poison the catalytic process and even permanently disable the catalytic converter [7]. In exploring the possibility of alternatives to precious metals for use in catalysis, it is therefore also important to explore how the most common air molecules and contaminants can affect the catalysis process, either positively or negatively. While few countries still use leaded fuel, and it will likely be phased out entirely around the world in the coming years, interaction by $H_2O$, $N_2$, and other common air molecules can never be eliminated, so it is especially important to explore how these molecules affect the catalysis process.

**1.2 Alternative Catalysts**

In 1987, Haruta *et. al.* [20] described the potential of gold nanoparticles to act as catalysts for the oxidation of carbon monoxide into carbon dioxide. It was found that supported gold nanoparticles were able to successfully oxidize carbon monoxide at temperatures as low as -70°C, even in high moisture conditions. This paper evoked great interest in the potential of small clusters of gold to act as a catalyst, particularly at ambient temperatures. Prestianni *et. al.* explored *CO* oxidation on neutral and cationic gold clusters, finding that *CO* oxidation occurs on cationic gold clusters when both *CO* and $O_2$ are adsorbed on the same site in the cluster [21]. Xing *et. al.* found that coadsorbed $H_2O$ enhanced the catalytic activity of gold cluster cations [22]. Further studies have been performed on clusters of the other coinage metals. Zhang *et. al.* found

silver clusters to be effective catalysts for $CO$ oxidation at low temperatures [23]. Hirabayashi found that copper anion clusters are also capable of oxidizing carbon monoxide [24].

In designing novel catalysts, it is important to note that effectiveness of a catalyst depends on a number of factors, including the phase of the catalyst relative to the reactants, its support, its size, and even its shape. For example, in automobile catalytic converters, the precious metals used as catalysts are commonly supported on a ceramic honeycomb structure designed to maximize surface area and withstand high temperatures [7]. An oxide, such as cerium oxide ($CeO_2$), is typically added to serve as an oxygen source for the necessary chemical reactions [7].

In practice, it can be difficult to isolate the effects of any one factor on the effectiveness of a catalyst. For this reason, it is useful to study the gas phase reactivity of single atoms, ions, or molecules, since external interactions such as solute-solvent and intermolecular interactions can be categorically excluded. Gas phase studies of atoms can additionally provide information about their reactivity, reaction mechanisms and rates, and thermochemistry, and also aid in identifying intermediates and key reaction steps controlling the catalytic activity. Therefore, even if the single atoms in gas phase are not by themselves capable of significant catalytic activity, gas phase studies can still offer useful information that will aid in the development of novel catalysts.

Many studies have also been performed on the gas phase reactions of single metal ions with molecules such as $CO$ and $H_2O$. Sato used the laser ablation-molecular beam (LAMB) method to calculate the binding energies of $Al^+$ and other monopositive metal ions to $H_2O$ [25]. Reveles *et. al.* found that single $Au^+$ ions are capable of $CO$ oxidation, though catalytic activity is inhibited by the presence of $H_2O$ [10]. Specifically, a number of studies have been performed on gas phase reactions of $Cu^+$ with various molecules. Jarvis *et. al.* studied the reaction of $Cu^+$ and other metal

cations with $CO$ and $O_2$ using inductively coupled plasma/selected-ion flow tube (ICPSIFT) tandem mass spectrometry and quantum chemical calculations [26]. Holland and Castleman measured the bond energies of complexes of $Cu^+$ and $NH_3$ and $H_2O$ using thermionic emission sources [27]. Rodgers *et. al.* studied the reaction of $Cu^+$ with $CO$, $O_2$, $CO_2$, $N_2$, $NO$, $N_2O$, and $NO_2$ using guided ion beam mass spectrometry [28]. The reaction of $Cu^+$ with $CO$ specifically has also been studied by Morgantini and Weber [29], Merchan *et. al.* [30], and Barnes *et. al.* [31].

# Chapter 2 - Theory

## 2.1 Schrodinger equation

The steady-state geometry and energy of any particle or collection of particles can be described by its wave function, which can be found by solving the Schrodinger equation in its time-independent form [32].

$$\hat{H}\Psi = E\Psi \tag{6}$$

For a collection of $N$ nuclei of mass $M$ with $n$ electrons of mass $m$, the Schrodinger equation is:

$$-\left[\sum_{A=1}^{N}\frac{\hbar^2}{2M_A}\nabla_A^2 - \frac{\hbar^2}{2m}\sum_{i=1}^{n}\nabla_i^2 + \frac{1}{4\pi\epsilon_0}\sum_{A=1}^{N}\sum_{B>A}^{N}\frac{Z_A Z_B}{R_{AB}} + \frac{1}{4\pi\epsilon_0}\sum_{i=1}^{n}\sum_{j>i}^{n}\frac{e^2}{r_{ij}} - \frac{1}{4\pi\epsilon_0}\sum_{A=1}^{N}\sum_{i=1}^{n}\frac{Z_A e^2}{R_{Ai}}\right]\Psi = E\Psi \tag{7}$$

The first two terms of the Hamiltonian represent the kinetic energy of the nuclei and electrons, respectively. The third term is the repulsive Coulombic potential energy between each pair of nuclei, and the fourth term is the repulsive Coulombic potential energy between each pair of electrons. The final term is the attractive Coulombic potential energy between each electron and each nucleus.

For this system, there are $N$ nuclear kinetic terms in the Hamiltonian, along with $n$ electron kinetic terms, $\frac{1}{2}N(N-1)$ nuclear potential terms, $\frac{1}{2}n(n-1)$ electronic potential terms, and $N \times n$ nuclear/electron potential terms. A simple triatomic molecule such as $Cu^+CO$ has 3 nuclei and 42 electrons, resulting in a Hamiltonian with a total of 1035 terms, of which 861 come from the interelectron potential.

For even larger systems, the number of terms increases exceedingly rapidly. This means that in practice, the Schrodinger equation for any system larger than a simple hydrogen atom is

impossible to solve analytically, and even to solve numerically with the aid of a computer requires a number of approximations and simplifications.

## 2.2 Born-Oppenheimer Approximation

The first approximation, used in molecular modeling of all kinds, is the Born-Oppenheimer approximation [33]. The nucleus of any atom is at minimum several thousand times more massive than its electrons (a copper nucleus, for example, is 115,000 times as massive as an electron). As a result, the electrons move much faster than the nuclei do and respond essentially instantaneously to nuclear motion [33]. For this reason, nuclear motion can be essentially ignored while calculating the electronic wave functions without much loss in accuracy. Using this assumption, it is possible to approximate the wave function as the product of separate nuclear and electronic wave functions [32].

$$\Psi = \Psi_{nuclei} \times \Psi_{electrons} \tag{8}$$

One can therefore focus on solving the electronic wave functions for any given nuclear position, which greatly simplifies the Schrodinger equation. The resulting Schrodinger equation for the electrons only is:

$$\left[ -\frac{\hbar^2}{2m} \sum_{j=1}^{n} \nabla_j^2 + \frac{1}{8\pi\epsilon_0} \sum_{j\neq i}^{n} \frac{e^2}{r_{ij}} - \frac{1}{4\pi\epsilon_0} \sum_{A=1}^{N} \sum_{i=1}^{n} \frac{Z_A e^2}{R_{Ai}} \right] \Psi_{electrons} = \hat{H}\Psi_{electrons} \tag{9}$$

However, since most systems have many more electrons than nuclei, the Born-Oppenheimer approximation does not by itself sufficiently simplify the Schrodinger equation to the point where it is easily solvable. For the example $Cu^+CO$ molecule, using the Born-

Oppenheimer approximation only reduces the number of terms in the Schrodinger equation from 1035 to 1029. More simplifications are needed before the problem becomes realistically solvable.

## 2.3 Electron Density and Hohenberg-Kohn Theorems

In reality, the wave function of the electrons is not of much interest, since it cannot actually be observed in practice. In addition, electrons are indistinguishable particles, so it is not useful to assign an individual wave function to each separate electron. A more valuable quantity to look at is the density of electrons as a function of their position; or, in other words, the probability of finding an electron at any given location. This electron density is related to the electronic wave function and is given by [34]:

$$\rho(\bar{r}) = 2 \sum_{i=1}^{n} \Psi_e^*(\bar{r}) \Psi_e(\bar{r}) \tag{10}$$

This equation gives the probability of finding any electron at position $\bar{r}$. The factor of two in front of the sum is present because the Pauli Exclusion Principle allows two electrons of opposite spins to occupy the same space.

The objective now is to rewrite the Schrodinger equation in terms of the electron density rather than the electronic wave function. Doing this will reduce the number of terms in the Schrodinger equation by a great deal and allow a numerical solution to be found with much less computing power needed. The electron density depends only on three spatial variables (*x, y, z*), while the wave function for *n* electrons depends on *3n* spatial variables (*x, y, z* for each electron) [34]. Using electron density in place of wave functions therefore reduces even the most complex system of atoms to one of only three dimensions.

In 1964, Pierre C. Hohenberg and Walter Kohn proved the two Hohenberg-Kohn theorems that relate electron density to the electron wave function. The first Hohenberg-Kohn theorem states that the ground state energy and the ground state electron density are related via a unique energy functional, given by [35]:

$$E[\rho(\bar{r})] = \int \rho(\bar{r})V_{ext}(\bar{r})d\bar{r} + F[\rho(\bar{r})] \qquad (11)$$

In this equation, $\rho(\bar{r})$ is the electron density, $V_{ext}(\bar{r})$ is the external potential (from the nuclei) under which the electrons move, and $F[\rho(\bar{r})]$ is an unknown functional that depends only on the electron density.

The second Hohenberg-Kohn theorem specifies that the true electron density is the electron density that minimizes the energy of the functional [35]. Therefore, if the functional is known, the electron density can be found variationally, that is by varying the electron density until an energy minimum is found. Once the energy minimum is found, the electron density can be accurately considered to be the true electron density [35].

What these two theorems show is that the electron density can indeed be used to solve the Schrodinger equation once the unique functional connecting the electron density to the electron wave function is known. Unfortunately, finding this functional and the corresponding electron density is not necessarily an easy process.

**2.4 Kohn-Sham Equations**

The two Hohenberg-Kohn theorems are not by themselves sufficient to solve the Schrodinger equation in terms of electron density because they do not offer a way to find the unique functional connecting the electron density to the wave function.

The Kohn-Sham equations resolve this problem by offering a way to approximate the functional $F[\rho(\bar{r})]$. It is approximated as the sum of three terms [36].

$$F[\rho(\bar{r})] = E_{KE}[\rho(\bar{r})] + E_H[\rho(\bar{r})] + E_{XC}[\rho(\bar{r})] \tag{12}$$

The first term, $E_{KE}[\rho(\bar{r})]$, is the kinetic energy of a system of noninteracting electrons with the same density as the real system in question.

$$E_{KE}[\rho(\bar{r})] = \sum_{i=1}^{n} \psi(\bar{r}) \left( -\frac{\hbar^2 \nabla^2}{2m} \right) \psi(\bar{r}) d\bar{r} \tag{13}$$

The second term, $E_H[\rho(\bar{r})]$, is the usual repulsive Coulombic energy between electrons, also known as the Hartree electrostatic energy.

$$E_H[\rho(\bar{r})] = \frac{1}{2} \frac{1}{4\pi\epsilon_0} \int \int \frac{\rho(\bar{r}_1)\rho(\bar{r}_2)}{|\bar{r}_1 - \bar{r}_2|} d\bar{r}_1 d\bar{r}_2$$

The final term, $E_{XC}[\rho(\bar{r})]$, is the exchange correlation energy, which includes the quantum mechanical exchange and correlation energies as well as the difference between the non-interacting kinetic energy of the first term and the true interacting kinetic energy of the real system [36].

The exchange correlation term can be calculated in many different ways, but a common method is to use the local density approximation. The local density approximation uses a uniform electron gas model, assuming that electron density is constant in space. The total exchange correlation energy can therefore be found by simple integration over all space [33].

$$E_{xc}[\rho(\bar{r})] = \int \rho(\bar{r}) \varepsilon_{xc}[\rho(\bar{r})] \tag{14}$$

In this equation, $\varepsilon_{XC}[\rho(\bar{r})]$ is the exchange correlation energy per electron which can be found using other methods, such as quantum Monte Carlo computations [33] or the analytical expressions proposed by Gunnarsson and Lundqvist [37].

Putting all terms together in equation 11, the total energy of the system is:

$$E[\rho(\bar{r})] = \int \rho(\bar{r})V_{ext}(\bar{r})d\bar{r} + \sum_{i=1}^{n} \psi(\bar{r})\left(-\frac{\hbar^2\nabla^2}{2m}\right)\psi(\bar{r})d\bar{r}$$

$$+\frac{1}{2}\frac{1}{4\pi\epsilon_0}\int\int\frac{\rho(\bar{r}_1)\rho(\bar{r}_2)}{|\bar{r}_1-\bar{r}_2|}d\bar{r}_1 d\bar{r}_2 + E_{XC}[\rho(\bar{r})]$$

(15)

A final step is to insert the nuclear-electron potential into the first term, and sum over all *N* nuclei.

$$E[\rho(\bar{r})] = \frac{1}{4\pi\epsilon_0}\sum_{=1}^{N}\int\frac{Z_A\rho(\bar{r})}{|\bar{r}-\bar{R}_{Ai}|}d\bar{r} + \sum_{i=1}^{n}\psi_i(\bar{r})\left(-\frac{\hbar^2\nabla^2}{2m}\right)\psi_i(\bar{r})d\bar{r}$$

$$+\frac{1}{2}\frac{1}{4\pi\epsilon_0}\int\int\frac{\rho(\bar{r}_1)\rho(\bar{r}_2)}{|\bar{r}_1-\bar{r}_2|}d\bar{r}_1 d\bar{r}_2 + E_{XC}[\rho(\bar{r})]$$

(16)

The electron density $\rho(\bar{r})$ can now be written in terms of a set of one-electron orbitals.

$$\rho(\bar{r}) = \sum_{i=1}^{n}|\psi_i(\bar{r})|^2$$

(17)

The Kohn-Sham equations can now be written.

$$\left[-\frac{\hbar^2}{2m}\nabla^2 + V(\bar{r}) + V_H(\bar{r}) + V_{XC}(\bar{r})\right]\psi_i(\bar{r}) = \varepsilon_i\psi_i(\bar{r})$$

(18)

Here, the three potential terms (nuclear/electron, electron/electron, and exchange-correlation) have been replaced by $V(\bar{r})$, $V_H(\bar{r})$, and $V_{XC}(\bar{r})$ respectively. This equation resembles the original Schrodinger equation after the Born-Oppenheimer approximation (equation 9), except instead of a summation over *n* electrons, there are *n* separate equations, one for each electron.

The Kohn-Sham equations are solved using a self-consistent method. The individual electron wave functions are written as a linear combination of orbitals, $\phi_j$.

$$\psi_i(\bar{r}) = \sum_j C_j\phi_j$$

(19)

Gaussian type orbitals (GTO) and Slater type orbitals (STO) are common choices for $\phi_j$, but other options are possible. The electron wave functions are put into the Kohn-Sham equations

(equation 18) and a new wave function is produced. The process is continued until the wave function converges and an energy minimum is found.


## 2.5 Theoretical and Computational Method

Several initial geometries for all possible species were constructed and run through the deMon2k code [38] using the PBE99 functional [39] and a linear combination of Gaussian type orbitals (LCGTO), along with DZVP basis sets [40] and GEN-A2 auxiliary function sets [41]. A tight convergence criteria ($10^{-6}$) was used whenever possible, though loosened when necessary to find a stable result. Geometries were optimized using a quasi-Newton method in internal coordinates without symmetry constraints [42-43].

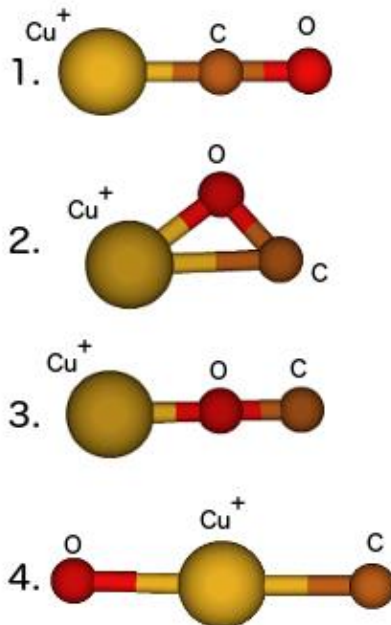To give an example, $Cu^+CO$ was run with the following four geometries:



**Figure 1**: Starting geometries of $Cu^+CO$.

14

Only geometries 1 and 3 were found to be stable, and geometry 1 was found to be of lower energy. The geometries corresponding to the lowest energies are considered the ground state geometries. To this the zero point energy correction was added. In addition, frequency analyses were conducted to verify the minima, and charge transfer analyses were conducted using the natural bonding orbital (NBO) method.

## 2.6 Experimental Method

The theoretical and computational results to follow are compared to experimental gas phase reactions of copper cations with molecules present in air, studied using Laser Vaporization Ionization High-Pressure Mass Spectrometry (LVI-HPMS) [44]. Copper cations were generated by focusing an Nd:YAG laser on a copper rod placed in a high pressure vacuum cell. The copper cations were then allowed to react with the intended molecules ($CO$, $O_2$, $H_2O$, and $N_2$) and stabilize through collisions with the helium carrier gas. The reaction products then exited the cell and were analyzed by a quadrupole mass filter [44].

Three different combinations of gas composition and pressure were used. The first gas consisted of pure $CO$ at 12, 35, and 100 mTorr; the second of pure $O_2$ at 12, 50, and 100 mTorr; and the final of a $CO/O_2$ (3.4%/20%) mixture at 12, 100, and 400 mTorr. In all cases, the gas mixtures also contained a small amount of impurities, including $H_2O$, $N_2$, and $O_2$ (in the case of pure $CO$) [44]. These gas mixtures reflect the composition of normal air, which at ground level contains mostly nitrogen ($N_2$) and oxygen ($O_2$), along with a certain amount water vapor ($H_2O$), depending on humidity.

# Chapter 3 - Results and Discussion

**3.1 Reactions of Cu$^+$ with CO, O$_2$, H$_2$O, and N$_2$**

**3.1.1 Reactions of Cu$^+$ with CO**

$Cu^+$ reacts with $CO$ successively to form $Cu^+CO$, $Cu^+(CO)_2$, $Cu^+(CO)_3$, and $Cu^+(CO)_4$ via the following reactions.

$$Cu^+ + CO \Leftrightarrow Cu^+(CO) \qquad\qquad \Delta E = -45.7 \; kcal/mol \qquad\qquad (20)$$

$$Cu^+CO + CO \Leftrightarrow Cu^+(CO)_2 \qquad\qquad \Delta E = -40.1 \; kcal/mol \qquad\qquad (21)$$

$$Cu^+(CO)_2 + CO \Leftrightarrow Cu^+(CO)_3 \qquad\qquad \Delta E = -19.6 \; kcal/mol \qquad\qquad (22)$$

$$Cu^+(CO)_3 + CO \Leftrightarrow Cu^+(CO)_4 \qquad\qquad \Delta E = -14.9 \; kcal/mol \qquad\qquad (23)$$

The binding energy $\Delta E$ was calculated as: $\Delta E = \sum total\; energy\; of\; products - \sum total\; energy\; of\; reactants$. According to this definition, a larger $\Delta E$ implies a more favorable process.

Each of these reactions is exothermic, with the thermodynamic favorability of each addition of $CO$ decreasing as the molecule grows. $Cu^+(CO)_5$ was not found to be a stable species, nor was any product found with more than four ligands connected to the $Cu^+$ atom. The addition reactions are shown in Figure 2.



**Figure 2:** Summary of $Cu^+$ reactions with $CO$. Optimized geometries are shown with bond lengths in Angstroms. Yellow, brown, and red circles represent $Cu$, $C$, and $O$ atoms respectively.

Experimentally, all $Cu^+(CO)_n$ with $n = 1 - 4$ were found during the gas phase reactions of $Cu^+$ with pure $CO$. At low pressures (12 mTorr), only $Cu^+CO$ formed. At 35 mTorr, $Cu^+(CO)_2$ was additionally found. Only at the highest pressure of 100 mTorr were $Cu^+(CO)_3$ and $Cu^+(CO)_4$ produced, in addition to their precursors $Cu^+(CO)$ and $Cu^+(CO)_2$. The full results of the gas phase reactions of $Cu^+$ with pure $CO$ are shown in Figure 3.
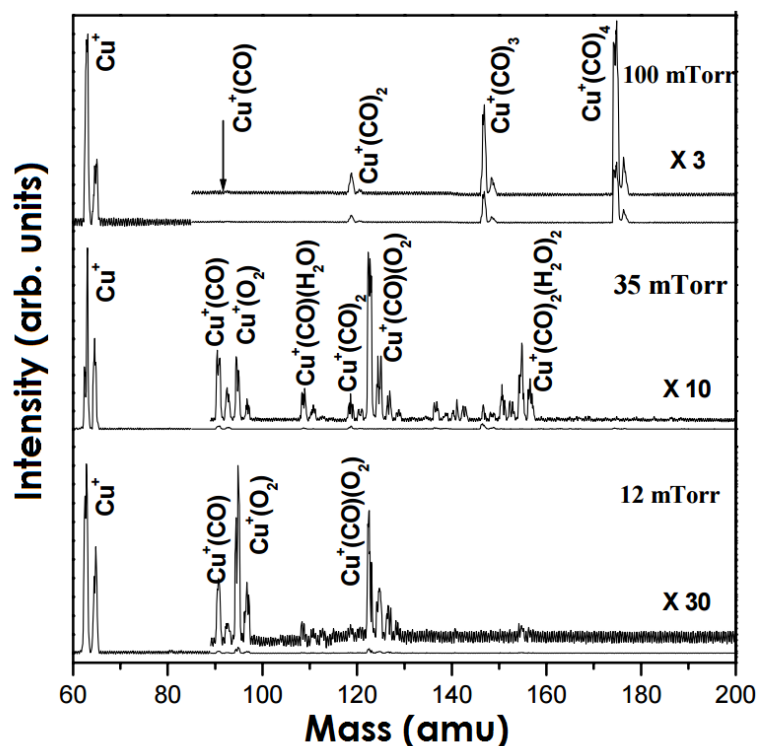


**Figure 3:** Mass spectrum of the gas phase reactions of $Cu^+$ with $CO$ [44].

By contrast, during the gas phase reactions of $Cu^+$ with the $CO/O_2$ mixture, only $Cu^+CO$ and $Cu^+(CO)_2$ were produced, and even then only at pressures of 100 mTorr and above. At 12, mTorr, only $Cu^+O$, $Cu^+O_2$, and $Cu^+(CO)O_2$ were produced, hinting at the competitive binding between $CO$ and $O_2$ on $Cu^+$. The full results of the gas phase reactions of $Cu^+$ with the $CO/O_2$ mixture are shown in Figure 4.
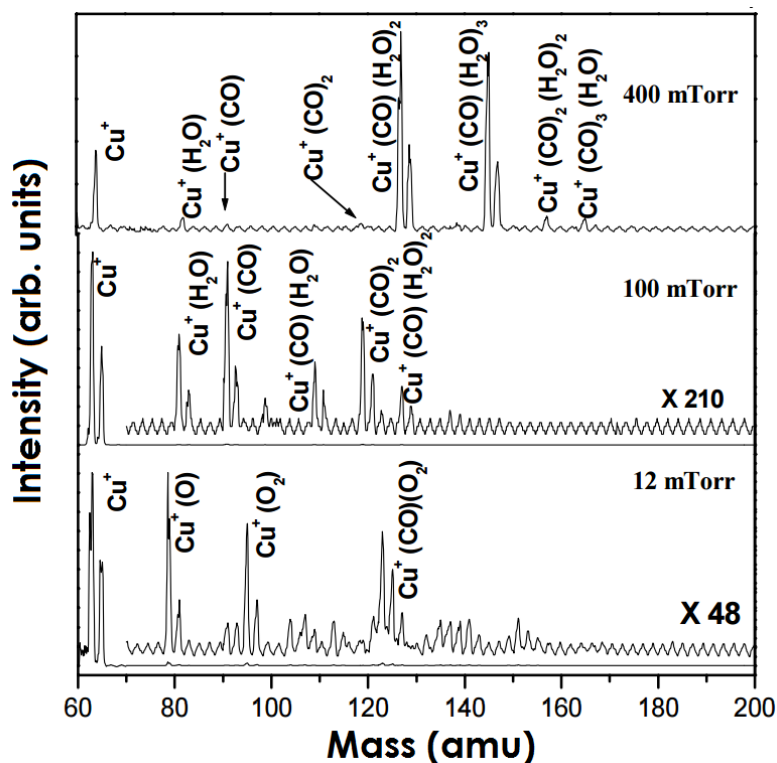
**Figure 4:** Mass spectrum of the gas phase reactions of $Cu^+$ with (3.4% $CO$, 20% $O_2$/$He$) mixture [44].

### 3.1.2 Reactions of $Cu^+$ with $O_2$

$Cu^+$ and $Cu^+CO$ can react with $O_2$ as shown in the following reactions:

$$Cu^+ + O_2 \Leftrightarrow Cu^+O_2 \qquad\qquad \Delta E = -19.8\ kcal/mol \qquad (24)$$

$$Cu^+CO + O_2 \Leftrightarrow Cu^+(CO)O_2 \qquad\qquad \Delta E = -17.1\ kcal/mol \qquad (25)$$

This last product, $Cu^+(CO)O_2$, is also possible as a result of $Cu^+O_2$ reacting with CO, as

shown in equation 26.

$$Cu^+O_2 + CO \Leftrightarrow Cu^+(CO)O_2 \qquad\qquad \Delta E = -42.9\ kcal/mol \qquad (26)$$

18

Both reactions produce the same geometry, as presented in Figure 5.
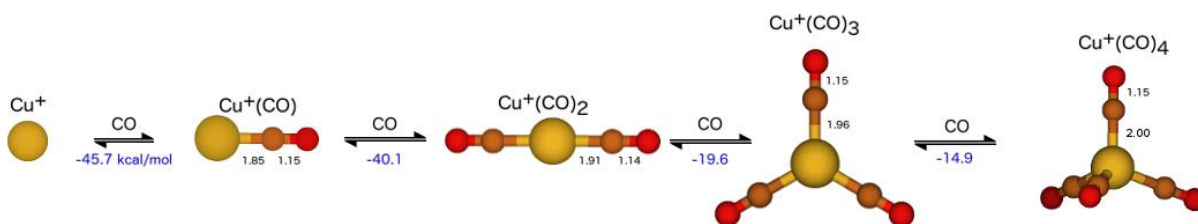


**Figure 5**: Summary of $Cu^+$ reactions with both CO and $O_2$. Optimized geometries are shown with bond lengths in Angstroms. Yellow, brown, and red circles represent Cu, C, and O atoms respectively.

No stable $Cu^+(O_2)_2$ product was found, which contradicts the findings of Jarvis *et. al.* [25]. This is likely because their pure $O_2$ reactions occurred at higher pressures.

Experimentally, $Cu^+O_2$ was found in all three gas mixtures, though only at pressures of 50 mTorr and below. The reactions with pure *CO* gas (Figure 3) resulted in $Cu^+O_2$ formation at 12 and 35 mTorr, while those with pure $O_2$ gas (Figure 6) produced $Cu^+O_2$ at 12 and 50 mTorr. Finally, the $CO/O_2$ mixture (Figure 4) produced $Cu^+O_2$ only at 12 mTorr. In no case was $Cu^+(O_2)_2$ found, and in all cases $Cu^+O_2$ disappeared at higher pressures to be replaced by other products, mostly involving *CO* and/or $H_2O$.
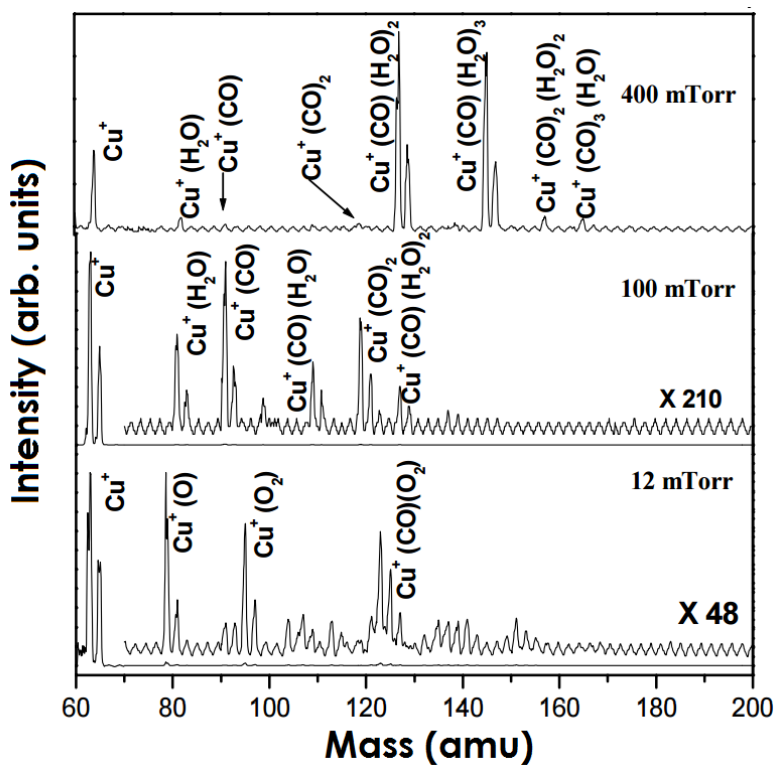
**Figure 6:** Mass spectrum of the gas phase reactions of $Cu^+$ with $O_2$ [44].

### 3.1.3 Reactions of $Cu^+$ with $H_2O$

$Cu^+$ reacts with $H_2O$ in successive reactions up to a maximum of three $H_2O$ ligands, forming $Cu^+(H_2O)$, $Cu^+(H_2O)_2$, and $Cu^+(H_2O)_3$.

$$Cu^+ + H_2O \Leftrightarrow Cu^+H_2O \qquad \Delta E = -43.6 \; kcal/mol \qquad (27)$$

$$Cu^+H_2O + H_2O \Leftrightarrow Cu^+(H_2O)_2 \qquad \Delta E = -40.9 \; kcal/mol \qquad (29)$$

$$Cu^+(H_2O)_2 + H_2O \Leftrightarrow Cu^+(H_2O)_3 \qquad \Delta E = -16.2 \; kcal/mol \qquad (29)$$

20

Only the first two $H_2O$ molecules attach directly to $Cu^+$. The third is connected to one of the other $H_2O$ molecules via hydrogen bond in the second coordination shell. The summary of $H_2O$ additions to $Cu^+$ is presented in Figure 7.
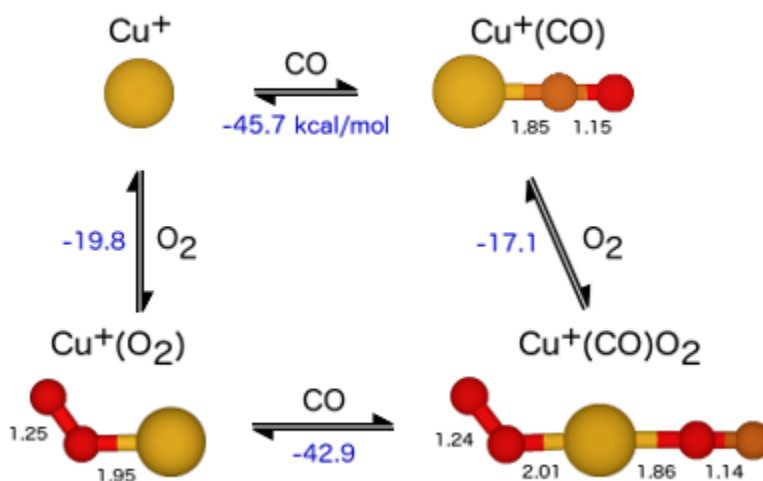


**Figure 7:** Summary of $Cu^+$ reactions with $H_2O$. Optimized geometries are shown with bond lengths in Angstroms. Yellow, red, and white circles represent $Cu$, $O$, and $H$ atoms respectively.

$Cu^+(CO)H_2O$ can also be formed by the reaction of $Cu^+H_2O$ with $CO$. Similarly, $Cu^+(CO)(H_2O)_2$ can also be formed by the reaction of $Cu^+(H_2O)_2$ with $CO$, and $Cu^+(CO)(H_2O)_3$ can be formed by the reaction of $Cu^+(H_2O)_3$ with $CO$. In each case, the geometry formed is the same as that formed by the first reaction.

$$Cu^+H_2O + CO \Leftrightarrow Cu^+(CO)H_2O \qquad \Delta E = -46.3 \ kcal/mol \qquad (30)$$

$$Cu^+(H_2O)_2 + CO \Leftrightarrow Cu^+(CO)(H_2O)_2 \qquad \Delta E = -25.0 \ kcal/mol \qquad (31)$$

$$Cu^+(H_2O)_3 + CO \Leftrightarrow Cu^+(CO)(H_2O)_3 \qquad \Delta E = -23.8 \ kcal/mol \qquad (32)$$

$Cu^+(CO)_2$ can react with up to two $H_2O$ molecules to form $Cu^+(CO)_2H_2O$ and $Cu^+(CO)_2(H_2O)_2$.

$$Cu^+(CO)_2 + H_2O \Leftrightarrow Cu^+(CO)_2H_2O \qquad \Delta E = -23.1 \ kcal/mol \qquad (33)$$

$$Cu^+(CO)_2H_2O + H_2O \Leftrightarrow Cu^+(CO)_2(H_2O)_2 \qquad \Delta E = -15.2 \ kcal/mol \qquad (34)$$

$Cu^+(CO)_2H_2O$ can also be a result of $Cu^+(CO)H_2O$ reacting with $CO$, and $Cu^+(CO)_2(H_2O)_2$ can also be a result of $Cu^+(CO)(H_2O)_2$ reacting with $CO$.

$$Cu^+(CO)H_2O + CO \Leftrightarrow Cu^+(CO)_2H_2O \qquad \Delta E = -18.9 \; kcal/mol \qquad (35)$$

$$Cu^+(CO)(H_2O)_2 + CO \Leftrightarrow Cu^+(CO)_2(H_2O)_2 \quad \Delta E = -14.5 \; kcal/mol \qquad (36)$$

Finally, $Cu^+(CO)_3H_2O$ can be formed either by a reaction of $Cu^+(CO)_3$ with $H_2O$ or a reaction of $Cu^+(CO)_2H_2O$ with $CO$.

The summary of all reactions involving $CO$ and $H_2O$ is given in Figure 8.
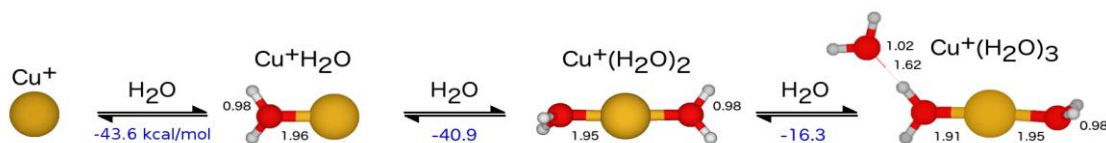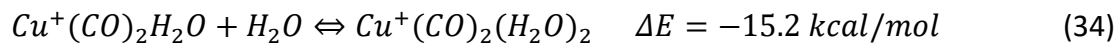


**Figure 8**: Summary of $Cu^+$ reactions with $CO$ and $H_2O$. Optimized geometries are shown with bond lengths in Angstroms. Yellow, brown, red, and white circles represent $Cu$, $C$, $O$, and $H$ atoms respectively.
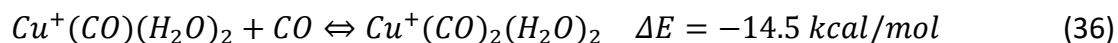
$H_2O$ was present as a contaminant in each of the gas tanks (pure $CO$, pure $O_2$, and $CO/O_2$ mixture). In the pure $CO$ case (Figure 3), only $Cu^+(CO)(H_2O)$ and $Cu^+(CO)_2(H_2O)_2$ were produced,

and only at 35 mTorr. Of note, neither $Cu^+(CO)_2(H_2O)$ nor $Cu^+(CO)(H_2O)_2$ were found to be present, though one of them must be the precursor to $Cu^+(CO)_2(H_2O)_2$, which was produced.

Reacting with pure $O_2$ (Figure 6), $Cu^+H_2O$ was produced at 12 and 100 mTorr, and $Cu^+(H_2O)_2$ was produced at 100 mTorr. In addition, $Cu^+(N_2)H_2O$ was found at 100 mTorr. No combination of $Cu^+$ with both $H_2O$ and $O_2$ was found experimentally.

The $CO/O_2$ mixture (Figure 4) produced a wider variety of products involving $H_2O$. $Cu^+H_2O$ was produced at each pressure, but $Cu^+(H_2O)_2$ was not found to be present at any pressure. Instead, a variety of combinations of $H_2O$ molecules and $CO$ molecules were formed, particularly at higher pressures. At 100 mTorr, $Cu^+(CO)H_2O$ and $Cu^+(CO)(H_2O)_2$ were found, while at 400 mTorr, each of those and in addition $Cu^+(CO)_2(H_2O)_2$, $Cu^+(CO)(H_2O)_3$, and $Cu^+(CO)_3H_2O$ were produced. $Cu^+(H_2O)_3$ was not found to be produced at any pressure in any gas mixture.

### 3.1.4 Reactions of $Cu^+$ with $N_2$

$Cu^+$ can react with $N_2$ to form $Cu^+N_2$ and $Cu^+(N_2)_2$.

$$Cu^+ + N_2 \Leftrightarrow Cu^+N_2 \qquad\qquad \Delta E = -29.4 \; kcal/mol \qquad (37)$$

$$Cu^+N_2 + N_2 \Leftrightarrow Cu^+(N_2)_2 \qquad\qquad \Delta E = -28.2 \; kcal/mol \qquad (38)$$

In addition, $Cu^+N_2H_2O$ can be produced either due to $Cu^+H_2O$ reacting with $N_2$ or due to $Cu^+N_2$ reacting with $H_2O$.

$$Cu^+H_2O + N_2 \Leftrightarrow Cu^+N_2H_2O \qquad\qquad \Delta E = -29.9 \; kcal/mol \qquad (39)$$

$$Cu^+N_2 + H_2O \Leftrightarrow Cu^+N_2H_2O \qquad\qquad \Delta E = -44.1 \; kcal/mol \qquad (40)$$

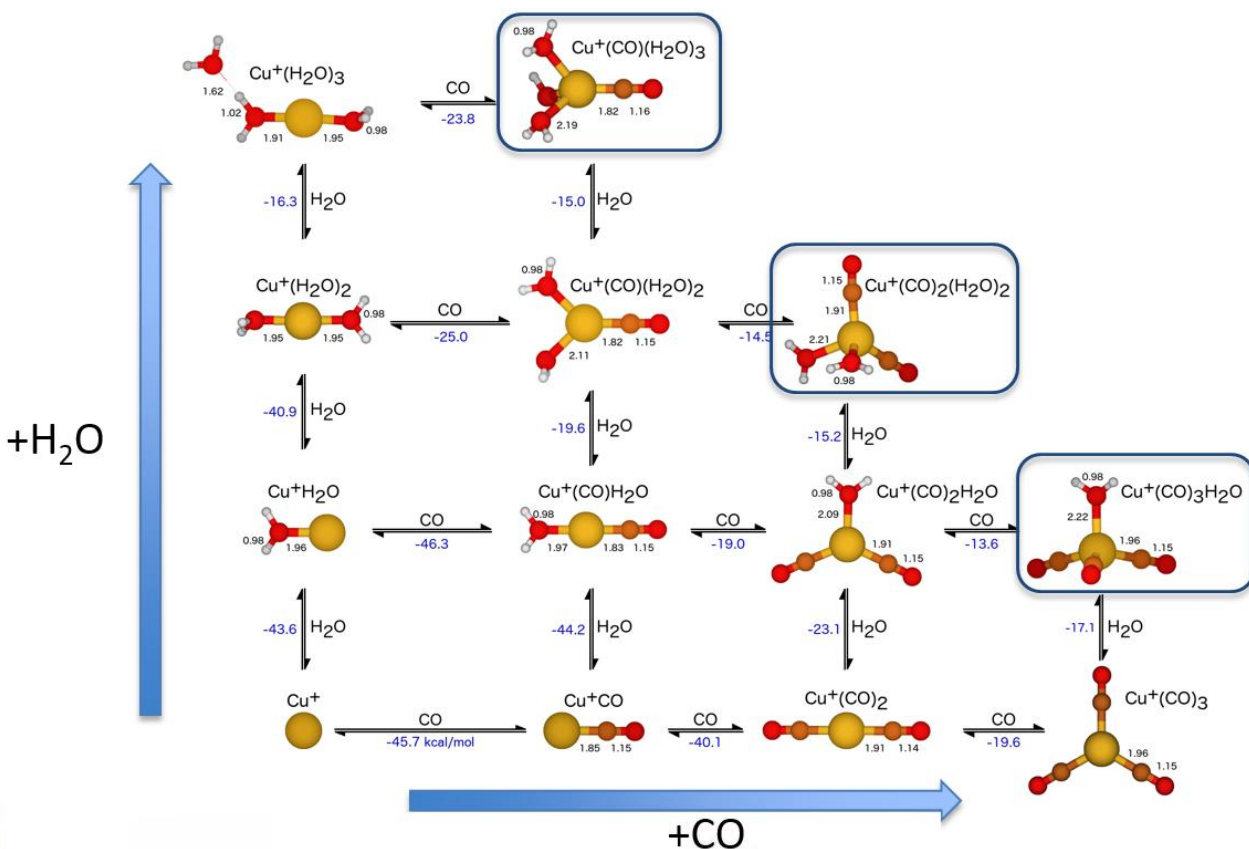A summary of $Cu^+$ reactions with $N_2$ and $H_2O$ is presented in Figure 9.
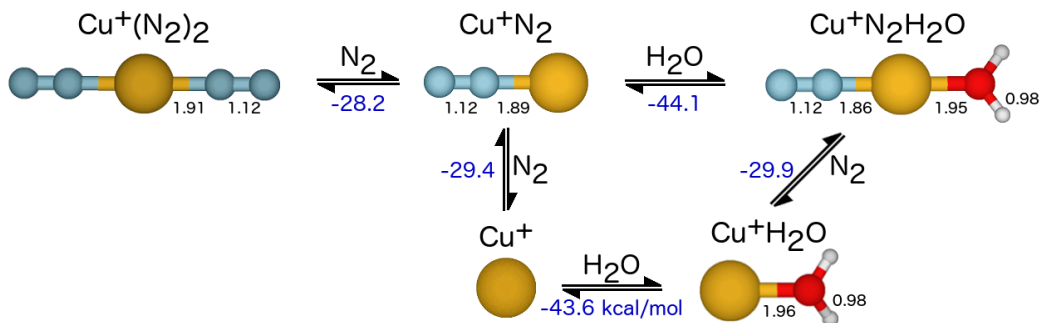
**Figure 9**: Summary of $Cu^+$ reactions with $H_2O$ and $N_2$. Optimized geometries are shown with bond lengths in Angstroms. Yellow, blue, red, and white circles represent $Cu$, $N$, $O$, and $H$ atoms respectively.

$Cu^+$ products with $N_2$ were found experimentally only in the gas phase reactions with pure $O_2$ (Figure 6), and was found only in combination with $H_2O$, never with $O_2$ or $CO$. $Cu^+N_2$ was found at each pressure, while $Cu^+(N_2)_2$ was found only at the highest pressure of 100 mTorr.

A summary of all possible reactions involving $CO$, $O_2$, $H_2O$, and $N_2$ is shown in Table 1.

| Pure CO Products | | | ΔE (kcal/mol) |
|---|---|---|---|
| $Cu^+$ + CO | → | $Cu^+(CO)$ | -45.6 |
| $Cu^+(CO)$ + CO | → | $Cu^+(CO)_2$ | -40.1 |
| $Cu^+(CO)_2$ + CO | → | $Cu^+(CO)_3$ | -19.6 |
| $Cu^+(CO)_3$ + CO | → | $Cu^+(CO)_4$ | -14.9 |

| Pure O$_2$ Products | | | ΔE (kcal/mol) |
|---|---|---|---|
| $Cu^+$ + $O_2$ | → | $Cu^+(O_2)$ | -19.8 |

| Pure H$_2$O Products | | | ΔE (kcal/mol) |
|---|---|---|---|
| $Cu^+$ + $H_2O$ | → | $Cu^+(H_2O)$ | -43.6 |
| $Cu^+(H_2O)$ + $H_2O$ | → | $Cu^+(H_2O)_2$ | -40.9 |
| $Cu^+(H_2O)_2$ + $H_2O$ | → | $Cu^+(H_2O)_3$ | -16.3 |

| Pure N$_2$ Products | | | ΔE (kcal/mol) |
|---|---|---|---|
| $Cu^+$ + $N_2$ | → | $Cu^+N_2$ | -29.4 |
| $Cu^+N_2$ + $N_2$ | → | $Cu^+(N_2)_2$ | -28.2 |

| CO/O$_2$ Products | | | ΔE (kcal/mol) |
|---|---|---|---|
| $Cu^+(CO)$ + $O_2$ | → | $Cu^+(CO)O_2$ | -17.1 |
| $Cu^+(O_2)$ + CO | | | -42.9 |

| CO/H$_2$O Products | | | |
|---|---|---|---|
| $Cu^+(CO)$ + $H_2O$ | → | $Cu^+(CO)H_2O$ | -44.3 |
| $Cu^+(H_2O)$ + CO | | | -46.3 |
| $Cu^+(H_2O)_2$ + CO | → | $Cu^+(CO)(H_2O)_2$ | -25.0 |
| $Cu^+(CO)H_2O$ + $H_2O$ | | | -19.6 |
| $Cu^+(CO)_3$ + H2O | → | $Cu^+(CO)_3H_2O$ | -17.1 |
| $Cu^+(CO)_2(H_2O)$ + CO | | | -13.6 |
| $Cu^+(CO)_2$ + $H_2O$ | → | $Cu^+(CO)_2H_2O$ | -23.1 |
| $Cu^+(CO)H_2O$ + CO | | | -18.9 |
| $Cu^+(CO)_2(H_2O)$ + $H_2O$ | → | $Cu^+(CO)_2(H_2O)_2$ | -15.2 |
| $Cu^+(CO)(H_2O)_2$ + CO | | | -14.5 |
| $Cu^+(CO)(H_2O)_2$ + $H_2O$ | → | $Cu^+(CO)(H_2O)_3$ | -15.0 |
| $Cu^+(H_2O)_3$ + CO | | | -23.8 |

| N$_2$/H$_2$O Products | | | ΔE (kcal/mol) |
|---|---|---|---|
| $Cu^+N_2$ + $H_2O$ | → | $Cu^+N_2H_2O$ | -44.1 |
| $Cu^+H_2O$ + $N_2$ | | | -29.9 |

Table 1: Summary of all possible reactions.

## 3.2 Competitive binding of *CO*, *H₂O*, *O₂*, and *N₂* to *Cu⁺*

According to the calculated results, *Cu⁺* binds strongest to *CO* (-45.7 kcal/mol), followed by *H₂O* (-43.6 kcal/mol), *N₂* (-29.4 kcal/mol), and *O₂* (-19.8 kcal/mol). After attaching the first *CO*,

$H_2O$ is energetically favored for the second ligand (-44.3 kcal/mol) over the addition of a second $CO$ molecule (-40.1 kcal/mol). Similarly, after the addition of the first $H_2O$ to $Cu^+$, $CO$ is energetically favored for the second ligand (-46.3 kcal/mol) over a second $H_2O$ molecule (-40.9 kcal/mol). Once two $CO$ molecules are bonded to $Cu^+$ in the form of $Cu^+(CO)_2$, the addition of $H_2O$ (-23.1 kcal/mol) to form $Cu^+(CO)_2H_2O$ is favored over the addition of another $CO$ molecule (-19.6 kcal/mol) to form $Cu^+(CO)_3$. Once three $CO$ molecules are bonded to the $Cu^+$ ion in $Cu^+(CO)_3$, it is again easier to bind an $H_2O$ molecule (-17.1 kcal/mol) to form $Cu^+(CO)_3H_2O$ than an additional $CO$ (-14.9 kcal/mol) to form $Cu^+(CO)_4$. The end result of this alternate adding of $CO/H_2O$ is that a large number of $Cu^+(CO)_n(H_2O)_m$ molecules with $n + m \leq 4$ are produced, particularly at higher pressures. This is confirmed experimentally, as shown in the mass spectrum of the $CO/O_2$ mixture in Figure 4.

Though $CO$ binds stronger to $Cu^+$ than does $O_2$, it is worth noting that $Cu^+O_2$ and $Cu^+(CO)O_2$ were both experimentally found in larger quantities than $Cu^+CO$ at low pressures of pure $CO$, as shown in the mass spectrum in Figure 3. At high pressures of pure $CO$ as well as in the $CO/O_2$ mixture, $Cu^+(CO)_n$ and $Cu^+(CO)_n(H_2O)_m$ products were found in larger amounts, and $Cu^+O_2$ and $Cu^+(CO)O_2$ disappeared entirely. This suggests that $O_2$ and $CO$ compete for spots on $Cu^+$, with $CO$ winning out at higher pressures to form $Cu^+(CO)_n$.

To investigate the reason for the difference in binding energies between the different species ($H_2O$, $O_2$, $CO$, and $N_2$), the charge transferred from the ligands to the $Cu^+$ ion was calculated, along with the HOMO-LUMO gap (the energy gap between the highest occupied and lowest unoccupied molecular orbitals). A higher HOMO-LUMO gap indicates a chemically more

stable complex, as the species must overcome a higher energy barrier to either give or receive electronic charge.

It was found that $Cu^+CO$ had the largest binding energy (-45.7 kcal/mol) as well as the largest HOMO-LUMO gap (3.60 eV). $Cu^+O_2$ had the lowest binding energy (-19.8 kcal/mol) and the lowest HOMO-LUMO gap (1.40 eV). However, while $Cu^+H_2O$ had a larger binding energy (-43.6 kcal/mol) than $Cu^+N_2$ (-29.4 kcal/mol), the latter had the larger HOMO-LUMO gap (3.00 eV compared to 2.16 eV for $Cu^+H_2O$).

In addition, $Cu^+$ received the largest charge reduction due to $CO$ adsorption (1.00$e$ to 0.93$e$), while its charge increased due to $O_2$ adsorption (1.00$e$ to 1.03$e$). The full summary of binding energies, electronic charge, electronic configuration, and HOMO-LUMO gaps are shown in Table 2.

| | ΔE (kcal/mol) | Electronic charge | Electronic Configuration | HOMO-LUMO gap (eV) |
|---|---|---|---|---|
| $Cu^+(CO)$ | -45.7 | **Cu: 0.93** | Cu [core] $4s^{0.26}3d^{9.81}$ | 3.6 |
| | | C: 0.35 | C [core] $2s^{1.43}2p^{2.16}$ | |
| | | O: -0.28 | O [core] $2s^{1.74}2p^{4.51}$ | |
| $Cu^+(H_2O)$ | -43.6 | **Cu: 0.94** | Cu [core] $4s^{0.16}3d^{9.89}$ | 2.2 |
| | | O: 1.05 | O [core] $2s^{1.75}2p^{5.28}$ | |
| | | H: 0.56 | H $1s^{0.44}$ | |
| | | H: 0.56 | H $1s^{0.44}$ | |
| $Cu^+N_2$ | -29.4 | **Cu: 1.00** | Cu [core] $4s^{0.15}3d^{9.85}$ | 3.0 |
| | | N: -0.25 | N [core] $2s^{1.56}2p^{3.64}$ | |
| | | N: 0.25 | N [core] $2s^{1.65}2p^{3.06}$ | |
| $Cu^+(O_2)$ | -19.8 | **Cu: 1.03** | Cu [core] $4s^{0.11}3d^{4.96}$ | 1.4 |
| | | O: -0.21 | O [core] $2s^{0.91}2p^{2.54}$ | |
| | | O: 0.18 | O [core] $2s^{0.92}2p^{2.52}$ | |
| $Cu^+(CO)O_2$ | -17.1/-42.9 | **Cu: 0.87** | Cu [core] $4s^{0.39}3d^{9.73}$ | 1.7 |
| | | C: 0.38 | C [core] $2s^{1.42}2p^{2.13}$ | |
| | | O: -0.29 | O [core] $2s^{1.74}2p^{4.52}$ | |
| | | O: -0.16 | O [core] $2s^{1.79}2p^{4.33}$ | |
| | | O: 0.19 | O [core] $2s^{1.83}2p^{3.95}$ | |

Table 2: Summary of binding energies, electronic charge, electronic configuration, and HOMO-LUMO gaps of $Cu^+ + M \rightarrow Cu^+M$ ($M = CO, H_2O, N_2, O_2$) and $(Cu^+CO + O_2)/(Cu^+O_2 + CO) \rightarrow Cu^+(CO)O_2$.

Of note is that significant charge transfer from $Cu^+$ to $O_2$ did not occur for the case of $Cu^+O_2$ or $Cu^+(CO)O_2$. For the Eley-Rideal mechanism of catalysis to work, once adsorbed as $Cu^+O_2$, the $O_2$ molecule must receive a significant amount of charge from the $Cu^+$ molecule, resulting in a stretching of the O-O bond due to partial filling of its highest occupied molecular orbital (HOMO), which is an antibonding orbital. As seen in Figure 5, the $O_2$ bond length in $Cu^+O_2$ is only

1.25 Å. This is only slightly longer than the free $O_2$ bond length of 1.21 Å [45]. Since little charge is transferred to the $Cu^+$ molecule and the $O_2$ bond length is not significantly stretched, it is unlikely that Eley-Rideal catalysis of $CO$ will occur. Similarly, when $CO$ and $O_2$ are coadsorbed on $Cu^+$ in $Cu^+(CO)O_2$, the $O_2$ bond is stretched only to 1.24 Å (Figure 5), and the $O_2$ molecule gains only a small amount of charge. For this reason, the Langmuir-Hinshelwood mechanism is equally unlikely to occur.

**3.3 Possible reactions producing $CO_2$**

Experimentally, $CO_2$ was not observed for any gas mixture at any pressure, either by itself or connected as a ligand to $Cu^+$ or another molecule. This, and the lack of $O_2$ activation shown by very little charge transfer to the $Cu^+$ molecule in $Cu^+O_2$ and $Cu^+(CO)O_2$ suggests that single $Cu^+$ ions are not by themselves capable of activating the $O_2$ molecule at room temperature.

Though $CO_2$ was not produced in the experiment, there are several pathways by which $CO_2$ could theoretically be produced.

1. A single $O$ atom can split off from $Cu^+(CO)O_2$ in an endothermic reaction.

$$Cu^+(CO)O_2 \Leftrightarrow Cu^+CO_2 + O \qquad\qquad \Delta E = 33.5 \; kcal/mol \qquad\qquad (41)$$

2. $Cu^+(CO)O_2$ can react exothermically with $CO$ to form $Cu^+CO_2$ and $CO_2$.

$$Cu^+(CO)O_2 + CO \Leftrightarrow Cu^+CO_2 + CO_2 \qquad\qquad \Delta E = -99.0 \; kcal/mol \qquad\qquad (42)$$

3. $O_2$ can react with $Cu^+(CO)_2$ to produce $Cu^+(CO)(CO_2)O$, which can then lose an oxygen atom to form $Cu^+(CO)CO_2$.

$$Cu^+(CO)_2 + O_2 \Leftrightarrow Cu^+(CO)(CO_2)O \qquad\qquad \Delta E = 101.6 \; kcal/mol \qquad\qquad (43)$$

$$Cu^+(CO)(CO_2)O \Leftrightarrow Cu^+(CO)CO_2 + O \qquad\qquad \Delta E = -91.3 \; kcal/mol \qquad\qquad (44)$$

4. Alternately, $Cu^+(CO)(CO_2)O$ can react with another $CO$ molecule to produce $Cu^+(CO)CO_2$ and $CO_2$.

$$Cu^+(CO)(CO_2)O + CO \Leftrightarrow Cu^+(CO)CO_2 + CO_2 \quad \Delta E = 223.9 \ kcal/mol \quad (45)$$
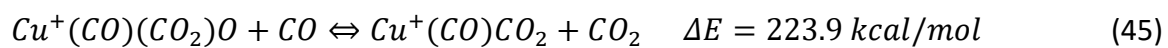
5. Finally, $Cu^+(CO)_3$ can react with $O_2$ to form $Cu^+(CO)(CO_2)_2$.

$$Cu^+(CO)_3 + O_2 \Leftrightarrow Cu^+(CO)(CO_2)_2 \quad\quad \Delta E = -111.1 \ kcal/mol \quad (46)$$

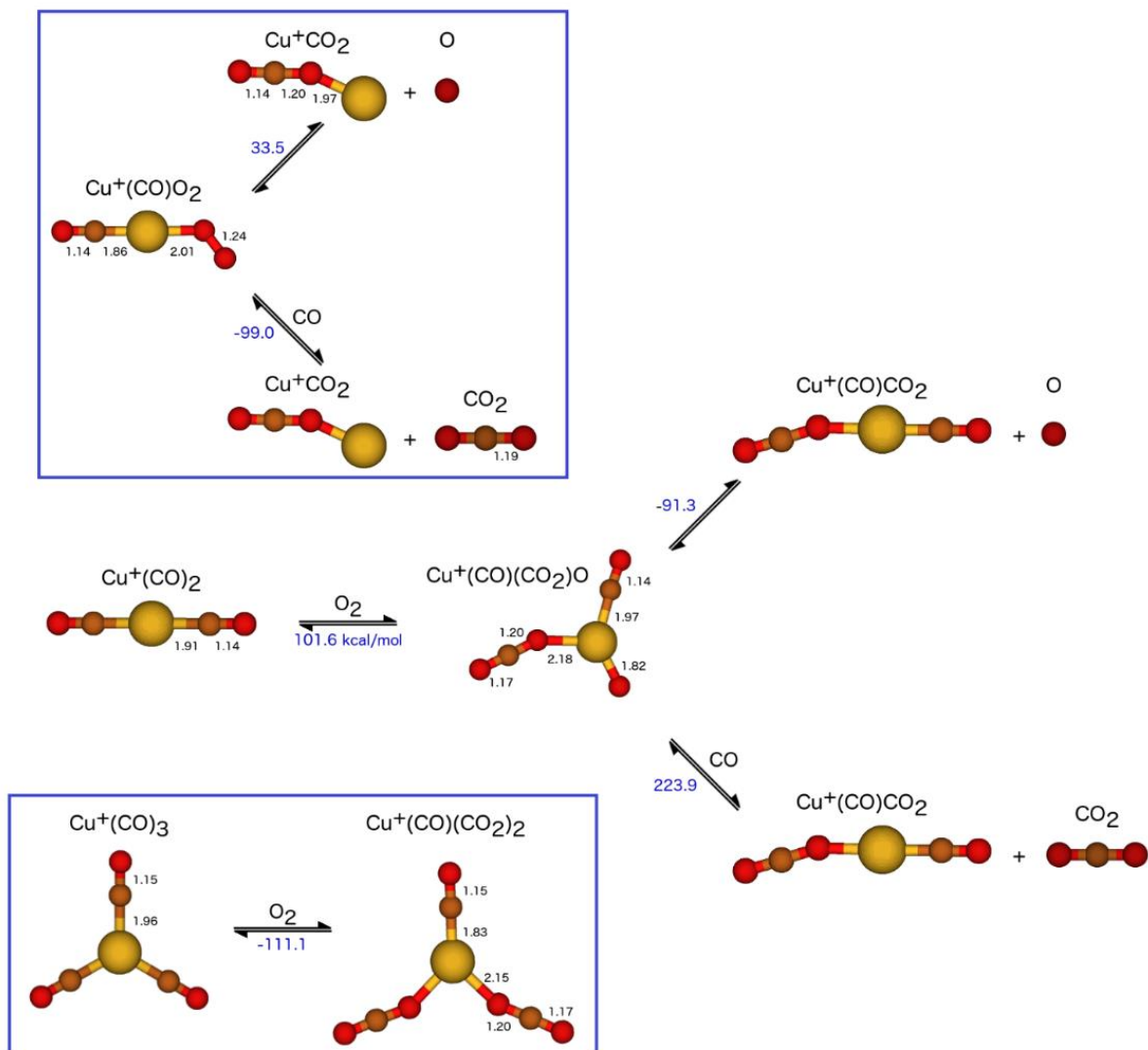A summary of these possible reaction pathways is shown in Figure 10.

**Figure 10**: Summary of possible $Cu^+$ with $CO/O_2$ mixture reactions resulting in the production of $CO_2$. Optimized geometries are shown with bond lengths in Angstroms. Yellow, brown, and red circles represent $Cu^+$, $C$, and $O$ atoms respectively.

Reactions 1, 3, and 4 are strongly endothermic, which makes it unlikely that they will occur at room temperature. Reactions 2 and 5 are exothermic, but they require the breaking of the unactivated O-O bond in the $O_2$ molecule. This requires a large activation energy which is unlikely to occur at room temperature.

It is useful to compare the reactions involving $Cu^+$ with $CO$, $O_2$, $N_2$, and $H_2O$ to a similar study on the theoretical gas phase reactivity of $Au^+$ with the same molecules performed by Reveles *et. al.* [10]. In this study, the $O_2$ bond was activated and $CO_2$ was produced. Copper and gold being both group 11 elements, they share many similar properties. Similar reactions are compared in Table 3.

| $Cu^+$ Reaction | Binding Energy (kcal/mol) | $Au^+$ Reaction | Binding Energy (kcal/mol) |
|---|---|---|---|
| $Cu^+ + CO \rightarrow Cu^+(CO)$ | -45.6 | $Au^+ + CO \rightarrow Au^+(CO)$ | -54.1 |
| $Cu^+(CO) + CO \rightarrow Cu^+(CO)_2$ | -40.1 | $Au^+(CO) + CO \rightarrow Au^+(CO)_2$ | -47.9 |
| $Cu^+(CO)_2 + CO \rightarrow Cu^+(CO)_3$ | -19.6 | $Au^+(CO)_2 + CO \rightarrow Au^+(CO)_3$ | -4.8 |
| $Cu^+ + O_2 \rightarrow Cu^+(O_2)$ | -19.8 | $Au^+ + O_2 \rightarrow Au^+(O_2)$ | -17.3 |
| $Cu^+(CO) + O_2 \rightarrow Cu^+(CO)O_2$ | -17.1 | $Au^+(CO) + O_2 \rightarrow Au^+(CO)O_2$ | -17.7 |
| $Cu^+ + H_2O \rightarrow Cu^+(H_2O)$ | -43.6 | $Au^+ + H_2O \rightarrow Au^+(H_2O)$ | -39.6 |
| $Cu^+(H_2O) + H_2O \rightarrow Cu^+(H_2O)_2$ | -40.9 | $Au^+(H_2O) + H_2O \rightarrow Au^+(H_2O)_2$ | -42.4 |
| $Cu^+(H_2O)_2 + H_2O \rightarrow Cu^+(H_2O)_3$ | -16.3 | $Au^+(H_2O)_2 + H_2O \rightarrow Au^+(H_2O)_3$ | -18.3 |
| $Cu^+(CO) + H_2O \rightarrow Cu^+(CO)H_2O$ | -44.3 | $Au^+(CO) + H_2O \rightarrow Au^+(CO)H_2O$ | -45.7 |
| $Cu^+(CO)H_2O + H_2O \rightarrow Cu^+(CO)(H_2O)_2$ | -19.6 | $Au^+(CO)H_2O + H_2O \rightarrow Au^+(CO)(H_2O)_2$ | -20.0 |
| $Cu^+(CO)_2 + H_2O \rightarrow Cu^+(CO)_2H_2O$ | -23.1 | $Au^+(CO)_2 + H_2O \rightarrow Au^+(CO)_2H_2O$ | -12.0 |
| $Cu^+(CO)_2(H_2O) + H_2O \rightarrow Cu^+(CO)_2(H_2O)_2$ | -15.2 | $Au^+(CO)_2(H_2O) + H_2O \rightarrow Au^+(CO)_2(H_2O)_2$ | -11.4 |
| $Cu^+ + N_2 \rightarrow Cu^+N_2$ | -29.4 | $Au^+ + N_2 \rightarrow Au^+N_2$ | -27.2 |
| $Cu^+N_2 + H_2O \rightarrow Cu^+N_2H_2O$ | -44.1 | $Au^+N_2 + H_2O \rightarrow Au^+N_2H_2O$ | -47.0 |
| $Cu^+(CO)(H_2O)_2 + H_2O \rightarrow Cu^+(CO)(H_2O)_3$ | -15.0 | $Au^+(CO)(H_2O)_2 + H_2O \rightarrow Au^+(CO)(H_2O)_3$ | -15.9 |
| $Cu^+(CO)_2 + O_2 \rightarrow Cu^+(CO)(CO_2)O$ | 101.6 | $Au^+(CO)_2 + O_2 \rightarrow Au^+(CO)_2O_2$ | -2.7 |
| $Cu^+(CO)(CO_2)O + CO \rightarrow Cu^+(CO)(CO_2) + CO_2$ | 223.9 | $Au^+(CO)_2O_2 + CO \rightarrow Au^+(CO)(CO_2) + CO_2$ | -115.0 |

Table 3: A comparison of the binding energies ($\Delta E$) for $Cu^+$ and $Au^+$ [10] with $CO$, $O_2$, $H_2O$, $N_2$, and their mixture.

$Cu^+$ and $Au^+$ perform similarly for all reactions with the exception of the last two, which are the ones lead to $CO_2$ production. In the $Cu^+$ case, $Cu^+(CO)_2$ reacts with $O_2$ to form $Cu^+(CO)(CO_2)O$, which then reacts with $CO$ to form $Cu^+(CO)CO_2$ and $CO_2$. These are both strongly

endothermic reactions. In the $Au^+$ case, $Au^+(CO)_2$ reacts with $O_2$ to form $Au^+(CO)_2O_2$ in a slightly

exothermic reaction, then $Au^+(CO)_2O_2$ reacts with $CO$ to form $Au^+(CO)CO_2$ and $CO_2$ in a strongly

exothermic reaction. Though the reactions involving $Au^+$ and $Cu^+$ are similar in many respect, $Au^+$

is able to produce carbon dioxide via a series of exothermic reactions, while a significant amount

of additional heat would be required to create carbon dioxide with $Cu^+$ as a catalyst.

# Chapter 4: Summary and Conclusions

An in depth theoretical investigation of the gas phase reactivity of $Cu^+$ with $CO$, $H_2O$, $O_2$, $N_2$ and their mixture demonstrates that $Cu^+$ interacts with all of the present ligands in competitive addition reactions until achieving saturation with four ligands. $CO$ binds strongest to $Cu^+$, followed by $H_2O$, $N_2$, and $O_2$. Though $Cu^+$ does bond to $O_2$, it does not result in the activation of the $O_2$ molecule (stretching of the O-O) bond. As a result, $CO_2$ production is not observed. The theoretical results are compared to experimental results and fit well together. The theoretical results for $Cu^+$ are also compared to a similar study done on $Au^+$ and the differences are compared. Though a single $Cu^+$ ion is not capable of activating $O_2$ and causing the production of $CO_2$, other studies have found that larger clusters of $Cu$ molecules are capable of activating $O_2$ and forming $CO_2$. Since moisture and other impurities can modify the chemical activity of catalysts, it is still useful to understand at the atomic level the interaction between these systems.

# References

1. J. Bierhals, in *Ullmann's Encyclopedia of Industrial Chemistry*, edited by Wiley-VCH Verlag GmbH & Co. KGaA (Wiley-VCH Verlag GmbH & Co. KGaA, Weinheim, Germany, 2001).

2. E.H. Smith, *Mechanical Engineer's Reference Book* (Elsevier Butterworth-Heinemann, Oxford, 2000), pp. 11/14.

3. K. Westberg, N. Cohen, and K.W. Wilson, Science **171**, 1013 (1971).

4. R.A. Silva, J.J. West, Y. Zhang, S.C. Anenberg, J.-F. Lamarque, D.T. Shindell, W.J. Collins, S. Dalsoren, G. Faluvegi, G. Folberth, L.W. Horowitz, T. Nagashima, V. Naik, S. Rumbold, R. Skeie, K. Sudo, T. Takemura, D. Bergmann, P. Cameron-Smith, I. Cionni, R.M. Doherty, V. Eyring, B. Josse, I.A. MacKenzie, D. Plummer, M. Righi, D.S. Stevenson, S. Strode, S. Szopa, and G. Zeng, Environ. Res. Lett. **8**, 034005 (2013).

5. P. Bharadwaj, J.G. Zivin, J.T. Mullins, and M. Neidell, Am. J. Respir. Crit. Care Med. **194**, 1475 (2016).

6. W.L. Beeson, D.E. Abbey, and S.F. Knutsen, Environ. Health Perspect. **106**, 813 (1998).

7. H. Yamagata, *The Science and Technology of Materials in Automotive Engines* (Woodhead Publishing Limited, 2005), pp. 228-247.

8. Intergovernmental Panel on Climate Change, editor , *Climate Change 2013 - The Physical Science Basis: Working Group I Contribution to the Fifth Assessment Report of the Intergovernmental Panel on Climate Change* (Cambridge University Press, Cambridge, 2014).

9. Y. Wang, G. Wu, M. Yang, and J. Wang, J. Phys. Chem. C **117**, 8767 (2013).

10. J.U. Reveles, K.M. Saoud, and M.S. El-Shall, Phys. Chem. Chem. Phys. **18**, 28606 (2016).

11. J.C. Prince, C. Trevino, and M. Diaz, *Proceedings of the World Congress on Engineering 2008, Vol II.* (IAENG, Hong Kong, 2008).

12. J. Heicklen, Ann. N. Y. Acad. Sci. **502**, 145 (1987).

13. United States Environmental Protection Agency. *Light-Duty Vehicles and Light-Duty Trucks: Clean Fuel Fleet Exhaust Emission Standards*. (2016).

14. National Research Council (U.S.) and National Academies (U.S.), *Global Sources of Local Pollution: An Assessment of Long-Range Transport of Key Air Pollutants to and from the United States* (National Academies Press, Washington, D.C, 2010), pp. 35 - 65.

15. M.J. Kirschner, in *Ullmann's Encyclopedia of Industrial Chemistry*, edited by Wiley-VCH Verlag GmbH & Co. KGaA (Wiley-VCH Verlag GmbH & Co. KGaA, Weinheim, Germany, 2000), pp. 637-645.

16. NASDAQ, "Platinum Price: Latest Price & Chart for Platinum," 22 Apr 2017, http://www.nasdaq.com/markets/platinum.aspx (23 Apr 2017).

17. NASDAQ, "Copper Price: Latest Price & Chart for Copper," 22 Apr 2017, http://www.nasdaq.com/markets/copper.aspx (23 Apr 2017).

18. D.M. Darst, *Portfolio Investment Opportunities in Precious Metals* (Wiley, Hoboken, New Jersey, 2013), pp. 47 - 54.

19. A. Luhn, "Where the river runs red: can Norilsk, Russia's most polluted city, come clean?", *The Guardian*, 15 Sep 2016, https://www.theguardian.com/cities/2016/sep/15/norilsk-red-river-russias-most-polluted-city-clean, (23 Apr 2017).

20. M. Haruta, T. Kobayashi, H. Sano, and N. Yamada, Chem. Lett. 75 (1987), pp. 405 - 408.

21. A. Prestianni, A. Martorana, F. Labat, I. Ciofini, and C. Adamo, J. Mol. Struct.: THEOCHEM **903**, 34 (2009).

22. X. Xing, X. Li, B. Yoon, U. Landman, and J.H. Parks, Int. J. Mass Spectrom. **377**, 393 (2015).

23. X. Zhang, Z. Qu, F. Yu, and Y. Wang, Chin. J. Catal. **34**, 1277 (2013).

24. S. Hirabayashi, Y. Kawazoe, and M. Ichihashi, Eur. Phys. J. D **67**, (2013).

25. H. Sato, Y. Horiki, and O. Ito, J. Photochem. Photobiol., A **92**, 17 (1995).

26. M.J.Y. Jarvis, L.F. Pisterzi, V. Blagojevic, G.K. Koyanagi, and D.K. Bohme, Int. J. Mass. Spectrom. **227**, 161 (2003).

27. P.M. Holland and A.W. Castleman, J. Chem. Phys. **76**, 4195 (1982).

28. M.. Rodgers, B. Walker, and P.. Armentrout, Int. J. Mass Spectrom. **182–183**, 99 (1999).

29. P. Morgantini and J. Weber, J. Mol. Struct. **166**, 247 (1988).

30. M. Merchan, I. Nebot-Gil, R. Gonzalez-Luque, and E. Orti, J. Chem. Phys. **87**, 1690 (1987).

31. L.A. Barnes, M. Rosi, and C.W. Bauschlicher, J. Chem. Phys. **93**, 609 (1990).

32. J.P. Lowe and K.A. Peterson, *Quantum Chemistry*, 3rd ed (Elsevier Academic Press, Burlington, MA, 2006).

33. A.R. Leach, *Molecular Modelling: Principles and Applications*, 2nd ed (Prentice Hall, Harlow, England ; New York, 2001).

34. D.S. Sholl and J.A. Steckel, *Density Functional Theory: A Practical Introduction* (Wiley, Hoboken, N.J, 2009).

35. P.P. Rushton, "The Hohenberg-Kohn Theorems", *Towards a Non-Local Density Functional Description of Exchange and Correlation*, Nov 2002, http://cmt.dur.ac.uk/sjc/thesis_ppr/node12.html, (22 Apr 2017).

36. P.P. Rushton, "The Kohn-Sham Formulation", *Towards a Non-Local Density Functional Description of Exchange and Correlation*, Nov 2002, http://cmt.dur.ac.uk/sjc/thesis_ppr/node13.html, (22 Apr 2017).

37. O. Gunnarsson, M. Jonson, and B.I. Lundqvist, Phys. Rev. B **20**, 3136 (1979).

38. G. Geudtner, P. Calaminici, J. Carmona-Espíndola, J.M. del Campo, V.D. Domínguez-Soria, R.F. Moreno, G.U. Gamboa, A. Goursot, A.M. Köster, J.U. Reveles, T. Mineva, J.M. Vásquez-Pérez, A. Vela, B. Zúñinga-Gutierrez, and D.R. Salahub, Wiler Interdiscip. Rev. Comput. Mol. Sci. **2**, 548 (2012).

39. B. Hammer, L.B. Hansen, and J.K. Nørskov, Phys. Rev. B: Condens. Matter Mater. Phys. **59**, 7413 (1999).

40. N. Godbout, D.R. Salahub, J. Andzelm, and E. Wimmer, Can. J. Chem. **70**, 560 (1992).

41. P. Calaminici, F. Janetzko, A.M. Köster, R. Mejia-Olvera, and B. Zuniga-Gutierrez, J. Chem. Phys. **126**, 044108 (2007).

42. J.U. Reveles and A.M. Köster, J. Comput. Chem. **25**, 1109 (2004).

43. J.U. Reveles, S.N. Khanna, and A.M. Köster, J. Mol. Struct.: THEOCHEM **762**, 171 (2006).

44. K.M.E. Saoud, Carbon Monoxide Oxidation on Nanoparticle Catalysts and Gas Phase Reactions of Small Molecules and Volatile Organics with Metal Cations, Virginia Commonwealth University, 2005.

45. W.M. Haynes, D.R. Lide, and T.J. Bruno, *CRC Handbook of Chemistry and Physics: A Ready-Reference Book of Chemical and Physical Data* (2016).